Hydrology Research

Hydrology Research Vol 53 No 2, 297 doi: 10.2166/nh.2022.076

Changes in actual evapotranspiration and its dominant drivers across the Three-River Source Region of China during 1982–2014

Jingkai Xie, Li Liu, Yitong Wang, Yue-Ping Xu* and Hao Chen

Institute of Hydrology and Water Resources, Civil Engineering, Zhejiang University, Hangzhou 310058, China
*Corresponding author. E-mail: yuepingxu@zju.edu.cn

JX, 0000-0001-5396-6456; YW, 0000-0001-5692-6214; HC, 0000-0001-9704-2781

ABSTRACT

Evapotranspiration is an essential element of the hydrological process. This study derived the long-term series of evapotranspiration from 1982 to 2014 over the three basins, namely source regions of the Yangtze River (SRYR), the Huang River (SRHR) and the Lancang River (SRLR) in the Three-River Source Region of China by integrating multiple sources of evapotranspiration estimates based on the Bayesian model averaging approach, which made full use of the strengths of land surface models and satellite-based products to constrain uncertainties. Then, we analyzed the influences of climate change on evapotranspiration based on the partial least squares regression model. Results indicate that (1) the agreement between various evapotranspiration products and water balance-derived evapotranspiration estimates varies from region to region in the Three-River Source Region of China; (2) annual evapotranspiration increases in the SRYR (3.3 ± 0.8 mm/yr) and the SRHR (0.8 ± 0.4 mm/yr), whereas no significant trends are observed in the SRLR during 1982–2014; (3) annual evapotranspiration is found most sensitive to precipitation and temperature in the SRYR and the SRHR, while it is dominated by relative humidity and temperature in the SRLR during 1982–2014. Our results have important implications for understanding evapotranspiration variability and future water security in the context of global climate change.

Key words: Bayesian model averaging (BMA), ET, partial least squares regression (PLSR), water balance method, the Three-River Source Region (TRSR)

HIGHLIGHTS

- Estimations of regional ET during the period of 2003–2014 are obtained by using the water balance method.
- Bayesian model averaging (BMA) is applied to merge multiple ET estimates with the goal of obtaining a long-term series of ET from 1982 to 2014.
- Dominant drivers of ET across the TRSR have been thoroughly analyzed based on a PLSR analysis.

1. INTRODUCTION

Evapotranspiration (ET) is one of the most essential elements in global water and energy cycles, which can play an important role in the process of hydrological cycles via a wide range of feedbacks acting on relative humidity, soil moisture and precipitation (Hu *et al.* 2018; Pascolini-Campbell *et al.* 2021). ET has long been viewed as the most difficult component to measure in hydrological cycles, because it is closely associated with the complex interactions within the land–plant–atmosphere system (Lemordant *et al.* 2018; Lian *et al.* 2018). In particular, it is difficult to estimate ET at regional scales in some high-mountain regions with limited meteorological stations, such as the Three-River Source Region (TRSR) of China (Figure 1), which are headwaters of many Asian rivers. Acting as a critical water reservoir, the TRSR of the Qinghai–Tibetan Plateau is an important source of fresh water for billions of people living in Asia. The water balance between ET and precipitation over this region can significantly influence the amount of water resources available in downstream regions and thus has a strong impact on future water security. Furthermore, this region is particularly sensitive to global climate change and plays an important role in the Asian climate because of its unique atmospheric circulation and high-altitude ecosystem (Immerzeel *et al.* 2010; Li *et al.* 2021b). In response to global warming, regional water circulation and hydrological processes over this region have been profoundly affected during the past decades (Wang *et al.* 2015; Xu *et al.* 2018a). Therefore, accurate ET

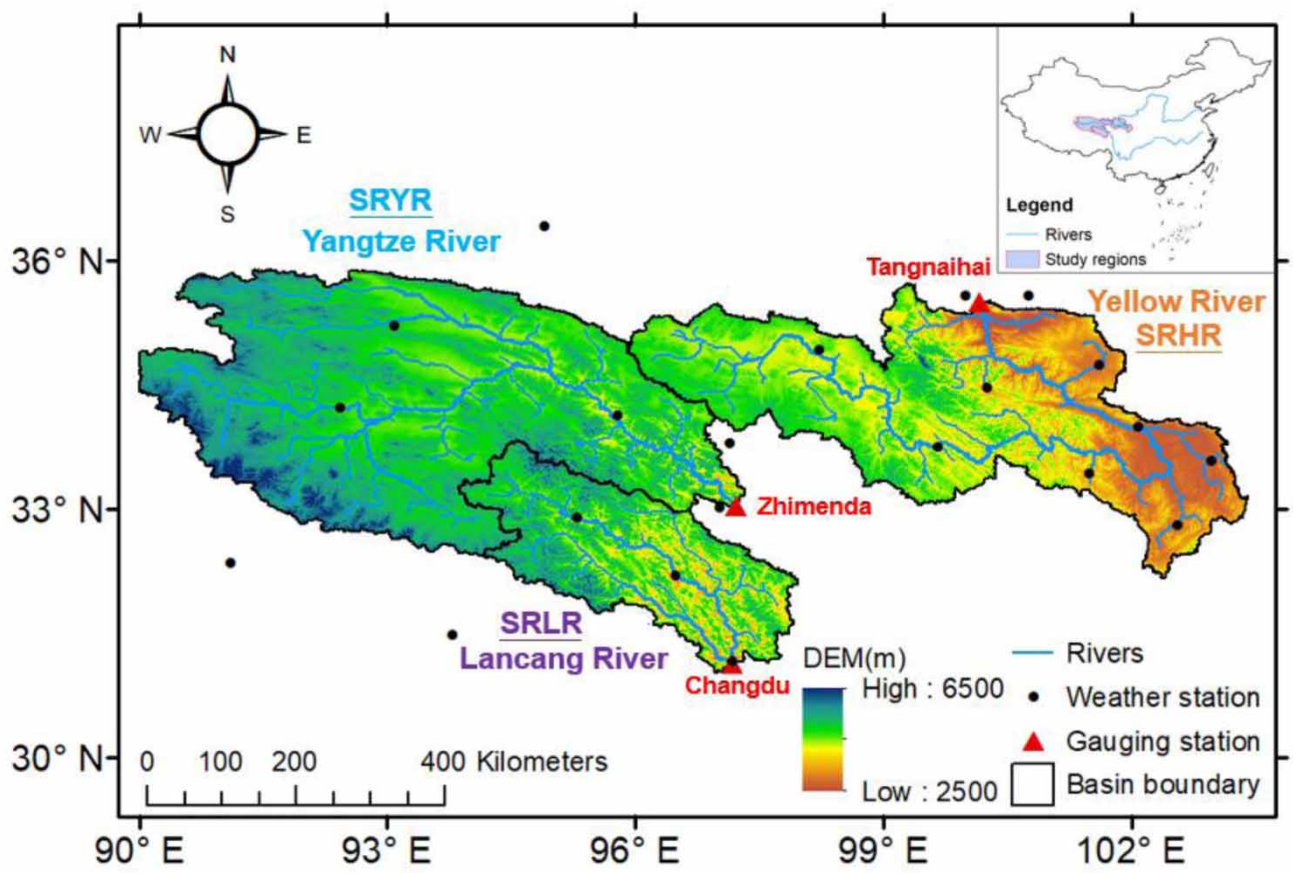

Figure 1 | Location of the Three-River Source Region (TRSR) of China, including the source regions of the Yangtze River (SRYR), the Huang River (Yellow; SRHR) and the Lancang River (SRLR); weather stations and runoff gauging stations.

estimates and the investigation of its sensitivities to climatic variables in the TRSR are crucial for water resource management and sustainable utilization.

Many studies have proposed different types of approaches to estimate regional ET, including remote sensing-based methods, land surface models and *in situ* measurements (e.g., FLUXNET eddy covariance towers, Bowen ratio energy balance). However, the inconsistency among various ET estimates is frequently found in previous studies (Liu *et al.* 2016; Pan *et al.* 2017), which can be mainly attributed to uncertainties in the meteorological variables and discrepancies in data processing. Since the successful launch of the Gravity Recovery and Climate Experiment (GRACE) satellite in 2002, some studies have attempted to calculate ET as a residual of the water balance equation by jointly using the GRACE data and hydro-meteorological data (mainly refer to precipitation and streamflow) (Billah *et al.* 2015; Xing *et al.* 2018). In comparison with traditional methods of estimating regional ET, the water balance method can effectively capture the true state of the hydrological process and has no requirements for extra forcing data, such as the type of land use, relative humidity and temperature, all of which are usually indispensable in hydrological models. To this end, this method has been regarded as one of the most optional methods to derive regional ET due to its great advantages.

The TRSR is located in the central region of the Qinghai–Tibet Plateau, which is also known as the 'Asia's water tower' (Immerzeel *et al.* 2010; You *et al.* 2020). The balance among ET, precipitation and runoff in this region can significantly influence downstream water availability. In addition, the cold region is an important area reflecting the complex interactions among soil, atmosphere and vegetation; therefore, variations in ET are of great importance for the water and energy balance for the TRSR under climate change. It has been widely acknowledged that the hydrological changes in cold regions are mostly attributed to global climate change (Zhao & Wu 2019; Shen *et al.* 2020). For example, various studies show that significant warming trends have been observed in the Qinghai–Tibet Plateau and the Tien Shan over the past decades, resulting in remarkable changes in regional hydrology, such as ET change and glacier shrinkage (Sorg *et al.* 2012; Wang *et al.* 2018;

Ma *et al.* 2019b). Previous study also noted that the spatial and temporal distributions of precipitation and temperature had clearly changed within the TRSR and its surrounding regions in recent years (Chu *et al.* 2019). However, long-term variation of ET, which can be significantly influenced by environmental changes, has been limitedly investigated in this region. Furthermore, few studies have fully analyzed the sensitivities of ET to climatic variables across the TRSR due to sparse gauging networks caused by its harsh environment.

Therefore, the present study mainly has three objectives: (1) to derive the regional ET based on the water balance method and evaluate the performances of different ET products in the TRSR; (2) to develop a long-term series of ET by merging different ET products and (3) to clarify the dominant factors of inter-annual variability in ET during the past decades. The rest of this paper is organized as follows. In Section 2, we make a brief introduction to the study region. Sections 3 and 4 describe the datasets and methods that are applied to analyze the changes in ET over the study region, respectively. Section 5 mainly includes the results and discussions regarding regional ET derived from the water balance method and long-term dynamics of ET by merging different ET products. Meanwhile, the sensitivities of annual ET to climatic variables across the TRSR have been fully investigated in this section. Finally, the conclusions drawn from this study are presented in Section 6.

2. STUDY AREA

The TRSR (31°12′–35°52′N, 89°54′–103°23′E) mainly includes the source regions of the Huang River (also termed the Yellow River; SRHR), the Yangtze River (SRYR) and the Lancang River (SRLR) (Figure 1). The Yangtze River and the Huang (Yellow) River are two major rivers in China and play a critical role in water supply, irrigation, as well as hydropower generation (Yu *et al.* 2014). The Lancang River is an important transboundary river in Asia, which provides fresh water to many Asian countries such as China, Burma, Laos, Thailand, Cambodia and Vietnam (Bonnema & Hossain 2019). The TRSR has a total area of approximately 330,000 km^2 with elevations ranging from 3,000 to 6,000 m (Table 1). Moreover, the ecological condition of this region is particularly sensitive to climate changes due to its high-altitude terrain and unique climate system, which could profoundly affect the terrestrial ecosystem and energy exchange in the Qinghai–Tibetan Plateau.

The TRSR belongs to a typical plateau continental climate, which is featured by strong solar radiation, two distinct seasons (wet and dry) and large diurnal variation in temperature. According to the observations from meteorological stations, the annual mean precipitation in the TRSR ranges from 450 to 590 mm with an average value of 540 mm, over 85% of which falls between May and September (Supplementary Figure S1). The annual runoff depth of this region ranges from 115 to 215 mm with a mean of 165 mm according to *in situ* observations acquired from Tangnaihai, Zhimenda and Changdu hydrological stations. In addition, the annual temperature ranges from −0.7 to 0.4 °C with an average of −0.3 °C. More detailed information about the distribution of meteorological stations and hydrological stations located in the TRSR is shown in Figure 1.

Table 1 | Detailed information about hydrological and meteorological variables over the three basins in the TRSR during 2003–2014

	Study regions			
Items	**TRSR**	**SRYR**	**SRHR**	**SRLR**
Location	90–103°E 31–36°N	90–97°E 32–36°N	96–103°E 32–36°N	94–98°E 31–34°N
Area (km^2)	334,032	157,025	122,729	54,278
Mean elevation (m)	4,502	4,778	4,128	4,556
Precipitation (mm/yr)	540	480	583	620
Runoff (mm/yr)	162	116	157	309
Runoff coefficient	0.3	0.24	0.27	0.49
Mean temperature (°C)	−0.3	−1.7	0.2	3.1
Hydrological station	–	Zhimenda	Tangnaihai	Changdu

Note. All the data sources for hydrological and meteorological variables included in this table are presented in Section 3. TRSR, Three-River Source Region; SRYR, Source Region of the Yangtze River; SRHR, Source Region of the Huang River; SRLR, Source Region of the Lancang River.

3. DATA

3.1. Typical long-term ET products

Although there are many types of ET products available for both hydrological and atmospheric communities, long-term ET products with high resolution are relatively few, especially in some large scale and remote regions such as the TRSR. To accurately characterize the long-term variations in ET in the TRSR, three high-resolution ET products are applied in this study, namely: (1) the newly published Global Land Evaporation Amsterdam Model Version 3.3a (GLEAM v3.3a) product with a 0.25°×0.25° resolution (hereafter ET_GLEAM) (Miralles *et al.* 2011a, 2011b; Martens *et al.* 2017); (2) the Global Land Data Assimilation System with Noah Land Surface Version 2.0 (GLDAS Noah v2.0) product with a 0.25°×0.25° resolution (hereafter ET_Noah) (Rodell *et al.* 2004) and (3) the ET products simulated by the latest complementary relationship (CR) with a 0.10°×0.10° resolution (hereafter ET_CR) (Ma *et al.* 2019a). ET_GLEAM and ET_Noah were generated by a land surface model and a remote sensing model, respectively, while ET_CR was estimated by using a calibration-free nonlinear complementary relationship. All these ET products have been widely used in different regions including the Qinghai–Tibetan Plateau due to the advantages of high resolution and reliability (Liu *et al.* 2020; Shi *et al.* 2020; Sun *et al.* 2021).

3.2. GRACE-derived TWSA

The GRACE satellites can provide monthly terrestrial water storage anomalies (TWSA) globally by measuring changes in Earth's gravity field. Therefore, three GRACE-derived mass concentration (mascon) solutions with a spatial resolution of 0.5°×0.5° are jointly used to detect the variations in TWSA in the TRSR, namely: (1) GRACE mascon solutions provided by the Center for Space Research (CSR, at the University of Texas, Austin) (Save *et al.* 2016); (2) GRACE mascon solutions provided by the Goddard Space Flight Center (GSFC, at NASA) (Awange *et al.* 2011) and (3) GRACE mascon solutions provided by the Jet Propulsion Laboratory (JPL, at NASA and California Institute of Technology, California) (Landerer & Swenson 2012).

In this study, the averages of these three monthly GRACE-derived mascon solutions are estimated to extract monthly TWSA in study regions (Tang *et al.* 2013; Xie *et al.* 2019a). Furthermore, terrestrial water storage changes (TWSC) at the monthly scale can be estimated as a result of the time derivative of TWSA. A few months of GRACE data are not available from 2003 to 2014 because of 'battery management'. All these missing data can be effectively interpolated from the previous and the next months, which has been proven useful and appropriate for perfectly maintaining the average seasonal cycle at the monthly scale (Long *et al.* 2015).

3.3. Meteorological data

Daily meteorological variables, including precipitation (P), sunshine duration (SSD), relative humidity (RHM) and temperature (T) from 1982 to 2014 are acquired from 21 National Meteorological Observatory stations. All these meteorological data are provided by the National Meteorological Information Center of the China Meteorological Administration (CMA) (http://data.cma.cn/). In light of the sparse distribution of meteorological stations in the TRSR (Figure 1), we also adopt another two high-resolution precipitation products besides the precipitation observations obtained from CMA in this study, namely: (1) China Gauge-based Daily Precipitation Analysis (CGDPA; Shen *et al.* 2010; Shen & Xiong 2016) and (2) Precipitation Estimation from Remotely Sensed Information using Artificial Neural Networks-Climate Data Record (PERISANN-CDR; Ashouri *et al.* 2016; Zhu *et al.* 2017).

3.4. *In situ* runoff observations

In situ runoff observations for several hydrological stations at the outlets of the three basins are obtained from the Yellow River Conservancy Commission of Ministry of Water Resources (http://www.yellowriver.gov.cn/other/hhgb/) and the Yangtze River Water Resources Commission of Ministry of Water Resource (http://www.cjw.gov.cn). Tangnaihai, Zhimenda and Changdu runoff gauging stations (Figure 1) have been chosen as the outlets of the SRHR, the SRYR and the SRLR, respectively. In addition, daily time series of *in situ* runoff observations are further aggregated into monthly values to keep consistent with the other items included in the water balance equation. More details of the datasets used in this study are presented in Table 2.

Table 2 | Datasets used in this study

Variables	Data sources	Temporal resolution	Spatial resolution	Period
TWSA	CSR Mascon	Monthly	0.5°	2002–2017
	JPL Mascon	Monthly	0.5°	2002–2017
	GSFC Mascon	Monthly	0.5°	2002–2017
ET	GLEAM	Monthly	0.25°	1982–2018
	GLDAS Noah	Monthly	0.25°	1948–2014
	CR	Monthly	0.1°	1982–2017
Runoff	*In situ*	Daily	–	2003–2014
Precipitation	CMA	Daily	–	1982–2014
	CGDPA	Daily	0.25°	1971–2014
	PERISANN-CDR	Daily	0.25°	1983–2014
Air temperature	CMA	Daily	–	1982–2014
Sunshine duration	CMA	Daily	–	1982–2014
Relative humidity	CMA	Daily	–	1982–2014

Note. TWSA, Terrestrial water storage anomalies; CSR, Center for Space Research; JPL, Jet Propulsion Laboratory; GSFC, Goddard Space Flight Center; GLEAM, Global Land Evaporation Amsterdam Model; GLDAS, Global Land Data Assimilation System; CR, Complementary Relationship; ET, Evapotranspiration. CGDPA, China Gauge-based Daily Precipitation Analysis; PERISANN-CDR, Precipitation Estimation from Remotely Sensed Information using Artificial Neural Networks-Climate Data Record. CMA, China Meteorological Administration.

4. METHODS

4.1. Terrestrial water storage change

By using GRACE data provided by three centers, monthly TWSC across the study region can be estimated by the double difference time derivative of TWSA (Ramillien *et al.* 2006; Long *et al.* 2013), which can be denoted as follows:

$$\mathrm{TWSC} = \frac{\mathrm{TWSA}(t+1) - \mathrm{TWSA}(t-1)}{2\Delta t} \tag{1}$$

where TWSC (mm) represents terrestrial water storage changes for month t across the study region; TWSA (t+1) (mm) and TWSA (t−1) (mm) represent terrestrial water storage anomalies for month (t+1) and month (t+1), respectively; Δt denotes the temporal sampling of GRACE-derived *TWSA*, which is taken as one month in this study.

4.2. Estimation of ET based on the water balance method

At basin scales, the water balance method has been viewed as the most appropriate method for estimating regional ET (Reager & Famiglietti 2013; Wan *et al.* 2015). Therefore, in this study, the water balance method is applied to estimate monthly time series of ET at a basin level based on the joint use of GRACE satellites and ground observations, that is,

$$\mathrm{ET} = P - R - \mathrm{TWSC} \tag{2}$$

where ET (mm) represents regional evapotranspiration estimated by the water balance method (hereafter ET_WB), P (mm) represents precipitation, R (mm) denotes basin outflow in depth, which mainly consists of surface water flow and groundwater flow; TWSC (mm) is terrestrial water storage changes for a given period, which can be acquired from Equation (1). To keep consistent with the temporal scale of GRACE-derived *TWSA*, all variables shown in the water balance equation are further processed and spatially averaged to obtain a monthly time-series data during the study period.

4.3. Bayesian model averaging for ET

Bayesian model averaging (BMA) is a popular approach to combine different models or forecasts, which can greatly improve the prediction accuracy of hydrological variables (Hoeting *et al.* 1999; Long *et al.* 2017). Rathinasamy *et al.* (2013) forecasted streamflow at different scales using a new BMA-based ensemble multi-wavelet Volterra approach and significantly increased the forecast accuracy. Chen *et al.* (2020) proposed a general BMA framework for merging sub-daily soil moisture products and improving their application in drought monitoring and prediction. In this study, the BMA approach is used to merge

three different ET products at basin scales, with the goal of improving the accuracy of ET estimation. The forecast probability density function (PDF) for ET is a weighted average of the PDFs for individual ET products (Madadgar & Moradkhani 2014; Baran *et al.* 2019), which can be expressed as follows:

$$p(y|f_1, f_2, \ldots, f_N) = \sum_{i=1}^{N} p(f_i|Y) \cdot p(y|f_i) \tag{3}$$

where $p(y|f_i)$ is the forecast PDF given a specific ET product f_i; Y is the reference ET that can be estimated by the water balance method during the training period; $p(f_i|Y)$ is defined as the posterior probability or the likelihood of the product f_i being correct given the reference ET Y. $p(f_i|Y)$ can be viewed as a statistical weight w_i that can reflect the performance of f_i in matching the reference ET Y during training period. Hence, Equation (3) also can be expressed as follows:

$$p(y|f_1, f_2, \ldots, f_N) = \sum_{i=1}^{N} w_i \cdot p(y|f_i) \tag{4}$$

where w_i denotes the statistical weight that is static for each ET product and $\sum_{i=1}^{N} w_i = 1$.

Assuming that $p(y|f_i)$ follows a Gaussian distribution with mean μ_i and variance σ_i^2 and can be denoted by $g(y|\theta_i)$, Equation (4) can be rewritten to describe the likelihood that a particular observation is predicted, that is,

$$p(y|f_1, f_2, \ldots, f_N) = \sum_{i=1}^{N} w_i \cdot g(y|\theta_i) \tag{5}$$

where g denotes the Gaussian distribution, $\theta_i = \{\mu_i, \sigma_i^2,\ i = 1, 2, \ldots, N\}$ is the vector of parameters.

The weight (w_i) and parameter vector (θ_i) of each ET product can be obtained by maximizing the log-likelihood function l, which can be expressed as follows:

$$l(\theta_i) = \sum_{s,t} \log\left(\sum_{i=1}^{N} w_i \cdot g(y_{s,t}|\theta_i)\right) \tag{6}$$

where $\theta_i = \{\mu_i, \sigma_i^2,\ i = 1,\ 2,\ \ldots, N\}$ is the vector of parameters; $\Sigma_{s,t}$ is the summation of observed ET from different products at basin s and time t; $y_{s,t}$ is an observed ET value for a specific basin s at time t.

Since the analytical solution to maximize the log-likelihood function l is complex, we maximize this function using the Expectation-Maximization (EM) algorithm as suggested by Raftery *et al.* (2005) and Duan *et al.* (2007). More details of BMA can also be found in the literature (Wöhling & Vrugt 2008; Lee *et al.* 2020).

In this study, a general approach that can effectively merge different ET products has been developed based on the BMA with the goal of deriving a long-term ET estimate. This approach can be carried out as follows. Firstly, we use the basin-scale water balance method to estimate monthly ET (ET_WB) during 2003–2014, which can be viewed as the reference ET in the following steps. Then, using GRACE-derived ET estimates based on the water balance method (ET_WB), three ET products including remote sensing-based GLEAM (ET_GLEAM), land surface model-based GLDAS Noah (ET_Noah) and complementary relationship-based CR (ET_CR), can be evaluated in each basin at monthly time scales relative to the reference ET. Meanwhile, the weight w_i of each ET product for the training period of 2003–2014 is obtained by the BMA approach. Finally, the obtained weight w_i is multiplied by the corresponding ET product to derive the long-term series of ET through the entire study period (1982–2014). The merged ET can be further applied to analyze the inter-annual variability of ET over the TRSR and its dominant drivers.

4.4. Partial least squares regression model

Partial least squares regression (PLSR) is a robust analytical tool that combines the features of multiple linear regression and principal component analysis (Abdi 2007; Yan *et al.* 2013). The PLSR has been widely used in hydrology studies because it can effectively address the problem of multi-collinearity among different predictors (Ma *et al.* 2015; Afriyie *et al.* 2020;

Ndehedehe & Ferreira 2020; Zhang & Wang 2021). As a result, this method can ensure that only significant components relevant to the response variable are retained when conducting regression (Shi *et al.* 2013). In this study, the partial least squares regression (PLSR) model is constructed to analyze the sensitivity of annual ET to different climatic variables across the study regions. In PLSR modeling, the estimated coefficients indicate the sensitivity of annual ET to different climatic variables for a specific basin. The terms with large coefficient values are the most relevant for explaining the variations in ET during the study period. Thus, it is possible to determine which climatic variables most strongly interact with ET during the study period by using the PLSR method. The detailed algorithm can be seen in Hu *et al.* (2021).

According to the findings revealed by previous studies, the regional ET is driven essentially by climatic variables (Gao *et al.* 2007; Cui *et al.* 2020; Xie *et al.* 2021). For example, Li *et al.* (2021a, 2021b) indicated that precipitation was the most important factor controlling ET changes over the entire water-limited regions in China. Soni & Syed (2021) indicated that precipitation was responsible for more than 65% of the ET changes observed in the Ganga River basins based on a Hierarchical Partitioning Analysis (HPA). Therefore, basin-averaged precipitation, temperature, sunshine duration and relative humidity have been selected as inputs, which are applied to analyze the dominant drivers of the inter-annual variation of ET based on the PLSR method in this work.

4.5. Performance metrics

In this study, evaluation criteria including correlation coefficient (r), root mean square error (RMSE), relative bias (BIAS) and the Kling-Gupta efficiency (KGE) are chosen to evaluate the performance of ET acquired from different products relative to that derived by the water balance method. These statistical metrics can be defined as:

$$r = \frac{\sum_{i=1}^{N}(x_i - \bar{x})(y_i - \bar{y})}{\sqrt{\sum_{i=1}^{N}(x_i - \bar{x})^2 \times \sum_{i=1}^{N}(y_i - \bar{y})^2}} \tag{7}$$

$$\mathrm{RMSE} = \sqrt{\frac{\sum_{i=1}^{N}(x_i - y_i)^2}{N}} \tag{8}$$

$$\mathrm{BIAS} = \frac{\sum_{i=1}^{N}(x_i - y_i)}{\sum_{i=1}^{N}(y_i)} \times 100\% \tag{9}$$

$$\mathrm{KGE} = 1 - \sqrt{(r-1)^2 + (\alpha - 1)^2 + (\beta - 1)^2} \tag{10}$$

where N represents the number of months during the study period; x_i represents the monthly ET estimated by the water balance method; y_i represents the monthly ET acquired from different products; $\bar{x}$ and $\bar{y}$ are the averages of monthly ET. For the KGE, r represents the linear correlation, α represents the variability bias and β represents the mean bias.

5. RESULTS AND DISCUSSION

5.1. Monthly time series of TWSA, TWSC, precipitation and runoff during 2003–2014

For all basins included in the TRSR, monthly time series of TWSA during 2003–2014 have been estimated by GRACE data from the three centers. As shown in Figure 2, there are large variations for TWSA and TWSC in different basins, especially for the SRYR. In general, regional TWSA shows an increase trend for the SRYR (2.2 ± 2.0 mm/yr, at the 95% confidence intervals) and the SRHR (1.9 ± 1.5 mm/yr, at the 95% confidence intervals), whereas it indicates a decreasing trend for the SRLR (-4.4 ± 1.7 mm/yr, at the 95% confidence intervals) during the period 2003–2014. This indicates that there exists obvious spatial heterogeneity in TWSA trends for the entire TRSR, reflecting the different hydrological responses to climate change in different regions. According to Equation (1), regional TWSC over the TRSR can be calculated from GRACE-derived TWSA, with a range from −24.5 to 41.4 mm/mon, −26.6 to 48.3 mm/mon and −20.0 to 32.1 mm/mon for the SRYR, the SRHR and the SRLR, respectively. Generally, monthly time series of TWSC across study regions exhibit an obvious seasonal

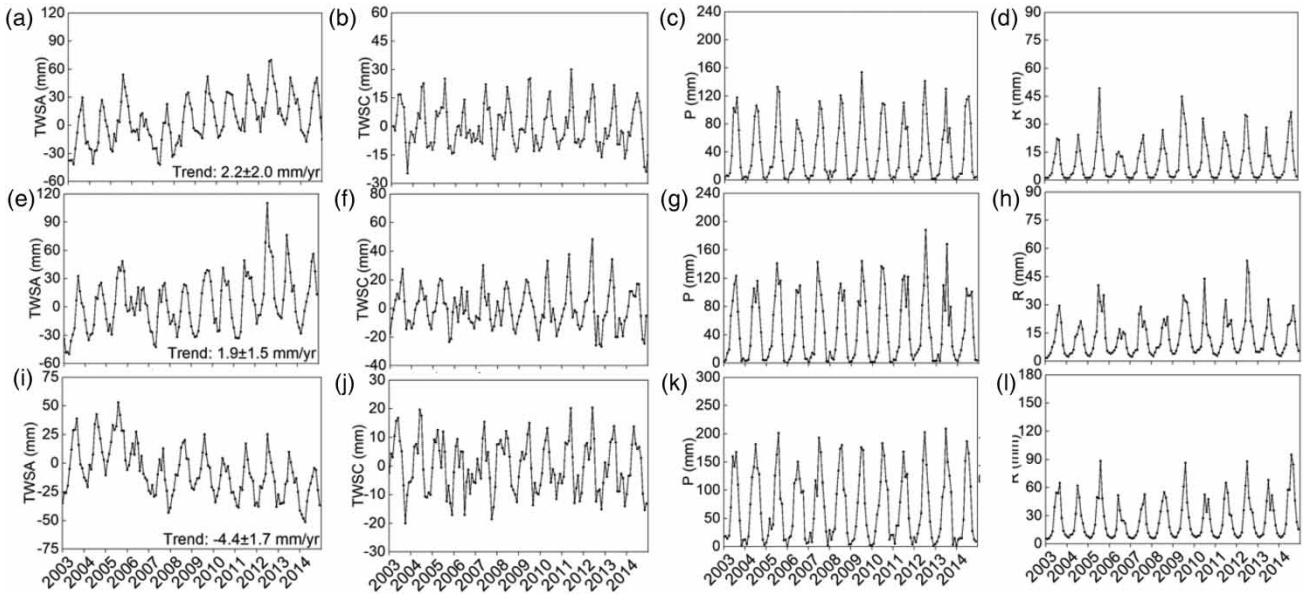

Figure 2 | Monthly time series of TWSA (mm), TWSC (mm), *P* (mm) and *R* (mm) in (a–d) the SRYR, (e–h) the SRHR and (i–l) the SRLR, respectively, from 2003 to 2014. TWSA, Terrestrial water storage anomalies; TWSC, Terrestrial water storage changes; *P*, Precipitation; *R*, Runoff; SRYR, Source region of the Yangtze River; SRHR, Source region of the Huang River; SRLR, Source region of the Lancang River.

cycle, showing a maximum value in summer (June to August) and a minimum value in winter (December to February) as expected.

5.2. Reference ET estimated by the water balance method during the training period (2003–2014)

In this study, we compute monthly times series of ET using the water balance method over the three basins in the TRSR, which overcomes the limitation of field observations due to its harsh environment and complex geophysical conditions. Figure 3 shows the comparison of monthly ET estimated by the water balance method and other three ET products during 2003–2014 which is a common period for all ET estimates. For the SRYR, ET_Noah is clearly lower than that estimated by the water balance method (i.e., ET_WB, shown in Figure 3) with a result of $BIAS=-48.30\%$, $r=0.91$ (shown in Table 3). Contrary to ET_Noah, monthly ET estimated by the complementary relationship (i.e., ET_CR) is generally higher than that of ET_WB in both low and high ends, with $BIAS=23.14\%$, $r=0.87$. In comparison, ET_GLEAM shows a better performance in matching ET_WB than the above two ET products, indicating $r=0.92$, $KGE=0.90$, $BIAS=-5.89\%$ and $RMSE=10.71$ mm/mon.

For the SRHR, the ET estimation simulated by GLDAS Noah most closely matches ET_WB among all three ET products with $r=0.90$ and $KGE=0.86$. In comparison, intra-annual variation of ET simulated by GLEAM is slightly different from ET_WB ($r=0.87$, $KGE=0.82$). It should be noted that ET_CR shows the largest discrepancy with ET_WB in the SRHR, indicating $r=0.85$, $KGE=0.66$, $BIAS=21.12\%$ and $RMSE=21.95$ mm/mon.

For the SRLR, ET_CR shows the smallest discrepancy with ET_WB among all three products at both low and high ends of the ET estimates, with $r=0.85$ and $KGE=0.81$. In addition, both ET_GLEAM and ET_Noah greatly underestimate seasonal variations of ET relative to ET_WB in this region, with relatively high biases ($BIAS=-21.34$ to -39.77%).

In summary, GRACE-derived ET estimates and that acquired from the various ET products show good agreements in the SRHR, whereas there are large discrepancies in the other two basins (i.e., the SRYR and the SRLR). This can be mainly attributed to the sparse distribution of meteorological stations for the SRYR and the SRLR (shown in Figure 1). Large uncertainties in forcing data that are caused by limited meteorological stations will inevitably lead to errors in ET estimates through the water balance method, which was also revealed by Xie *et al.* (2019b).

Using GRACE-derived ET estimates based on the water balance method (ET_WB), three ET products including remote sensing-based GLEAM (ET_GLEAM), a land surface model-based GLDAS Noah (ET_Noah) and the complementary relationship-based CR (ET_CR), can be evaluated in each basin at monthly time scales. In general, ET_GLEAM most closely

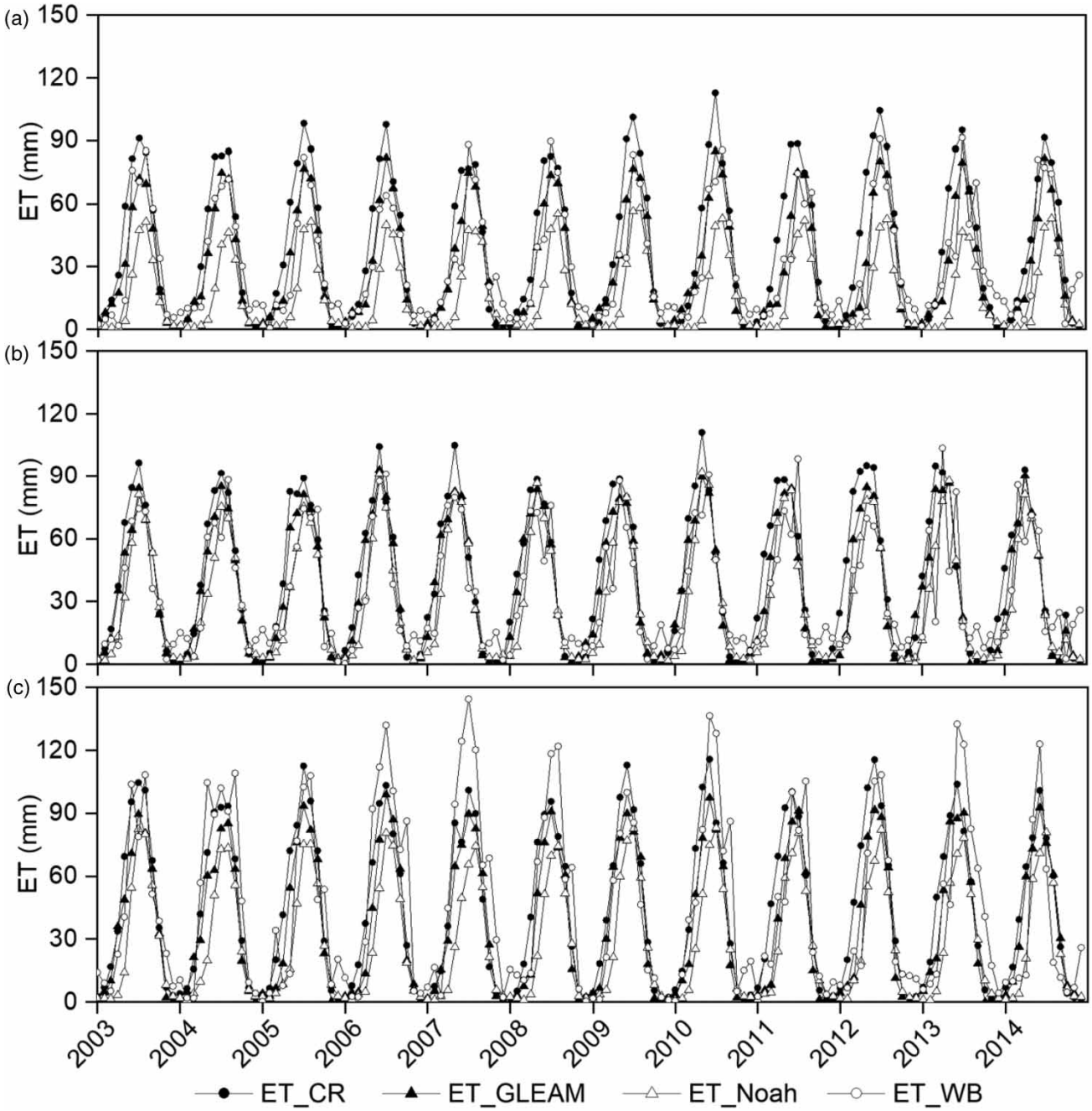

Figure 3 | Comparison of monthly ET estimated by the water balance method (ET_WB) and the other three ET products (ET_CR, ET_GLEAM and ET_Noah) over (a) the SRYR, (b) the SRHR and (c) the SRLR, respectively, from 2003 to 2014. ET, Evapotranspiration; SRYR, Source region of the Yangtze River; SRHR, Source region of the Huang River; SRLR, Source region of the Lancang River. ET_WB represents monthly evapotranspiration estimated by the water balance method; ET_GLEAM represents monthly evapotranspiration derived from the Global Land Evaporation Amsterdam Model Version 3.3a product; ET_Noah represents monthly evapotranspiration derived from the Global Land Data Assimilation System with Noah Land Surface Version 2.0 product; ET_CR represents monthly evapotranspiration derived from the datasets simulated by the latest complementary relationship.

matches with ET_WB among all three ET products, showing both relatively low *BIAS* (−21.34 to 5.78%) and *RMSE* (10.71–22.56 mm/mon), as well as good correlation ($r \geq 0.87$ and $KGE \geq 0.69$) over the three basins in the TRSR. ET_Noah generally underestimates seasonal variations in ET relative to GRACE-derived estimates to some degree, showing negative values of *BIAS* over all basins in the TRSR (SRYR: −48.3%; SRHR: −9.79%; SRLR: −39.77%). Contrary to ET_Noah, ET_CR

Table 3 | Evaluation metrics for ET acquired from different ET products (i.e., ET_CR, ET_GLEAM and ET_Noah) relative to that estimated by the water balance method (ET_WB) over the three basins in the TRSR

	SRYR			SRHR			SRLR		
Metrics	**ET_Noah**	**ET_CR**	**ET_GLEAM**	**ET_Noah**	**ET_CR**	**ET_GLEAM**	**ET_Noah**	**ET_CR**	**ET_GLEAM**
r	0.91	0.87	**0.92**	**0.90**	0.85	0.87	0.87	**0.85**	0.88
BIAS (%)	−48.30	23.14	**−5.89**	**−9.79**	21.17	5.78	−39.77	**−4.21**	−21.34
RMSE (mm)	19.08	18.28	**10.71**	**12.99**	19.24	15.23	28.42	**21.95**	22.56
KGE	0.42	0.63	**0.90**	**0.86**	0.66	0.82	0.48	**0.81**	0.69

Note. The most consistent performance for a specific basin is represented by the bold values. ET, Evapotranspiration; SRYR, Source region of the Yangtze River; SRHR, Source region of the Huang River; SRLR, Source region of the Lancang River. ET_WB represents monthly evapotranspiration estimated by the water balance method; ET_GLEAM represents monthly evapotranspiration derived from the Global Land Evaporation Amsterdam Model Version 3.3a product; ET_Noah represents monthly evapotranspiration derived from the Global Land Data Assimilation System with Noah Land Surface Version 2.0 product; ET_CR represents monthly evapotranspiration derived from the datasets simulated by the latest complementary relationship.

shows an overestimation of seasonal ET in all study regions except for the SRLR, which denotes a negative value of $BIAS = -4.21\%$. The *KGE* values shown in Table 3, considering cross-correlation, bias in the mean and bias in the variability, indicate that ET_GLEAM for the SRYR, ET_Noah for the SRHR and ET_CR for the SRLR are most consistent with GRACE-derived estimates during the study period. That is to say, one ET product may have a high performance at some sites but a poor performance at other sites. For example, ET_Noah has the largest bias over the SRYR and has the smallest bias over the SRHR. Furthermore, it also highlights the importance and necessity of developing a new approach to merge different ET estimations for improving the accuracy of regional ET.

Figure 4 plots the multi-year averages of monthly ET in 2003–2014 over the three basins included in the TRSR. All ET estimates show a typical unimodal distribution with the maximum in July and minimum in December or January, which can be attributed to the joint effects of precipitation and temperature (Supplementary Figure S1). According to ET_WB estimated by the water balance method, ET exhibits strong seasonality with more than 75% of annual ET occurring in the monsoon period (May to September) across the TRSR. In addition, there exist large discrepancies between water balance-derived ET and all ET products in terms of the magnitude of seasonal variations (Figure 4). For example, among all three ET products applied in this study, ET_Noah has the weakest seasonal ET variations while ET_CR has the strongest seasonal ET variations in study regions. This inconsistency in various ET estimates mainly arises from different model algorithms and processing methods.

5.3. Long-term series of ET during 1982–2014 by merging different ET products based on the BMA approach

Although monthly ET over the study regions can be estimated by using the water balance method, long-term series of ET are still not available due to a short period of GRACE data. To better understand the hydrological responses to climate change across the TRSR, long-term series of ET in this region should be further estimated. As a result, a general approach that can effectively merge different ET products has been developed with the goal of deriving a long-term ET estimate (described in Section 4.3).

The BMA algorithm assigns weights to each individual ET product based on *a priori* performance evaluation of these products in the common period (i.e., 2003–2014). Table 4 presents the weights w_i of each ET product over the study regions during 2003–2014, which reflects the contribution of each individual ET product in the BMA method. It can be seen that the BMA weights can vary a lot from region to region, implying that the relative contribution of each individual ET product to the ensemble of ET estimates is not the same in different regions. These weights are then assigned for the corresponding ET products during the entire period (i.e., 1982–2014) to generate an ensemble of ET estimates.

The BMA estimates of annual ET over the three basins in the TRSR are shown in Figure 5. For the SRYR, the estimated annual ET ranges from 281 to 401 mm during the 1982–2014 period (Figure 5(a)), showing a significantly increasing trend at a rate of 3.3 ± 0.8 mm/yr. A previous study (Li *et al.* 2014) has estimated the annual variation of ET for the SRYR and the SRHR during 1983–2006, showing an upward trend for annual ET in these two large basins. Liu *et al.* (2011) indicated that annual total ET in the SRYR showed a significant increasing trend at the 99% confidence level from 1980 to 2007. Compared to the SRYR, annual ET in the SRHR shows a lower variation range from 391 to 439 mm during the same period (Figure 5(b)), which is comparable to other estimates in the literature. For example, Xue *et al.* (2013) indicated that annual ET values were 306.6 and 359.7 mm in the SRYR and the SRHR, respectively, from 1982 to 2006 according to the water balance method. In addition, Xu *et al.* (2018a, 2018b) suggested that annual ET exhibited an increasing trend at a rate of

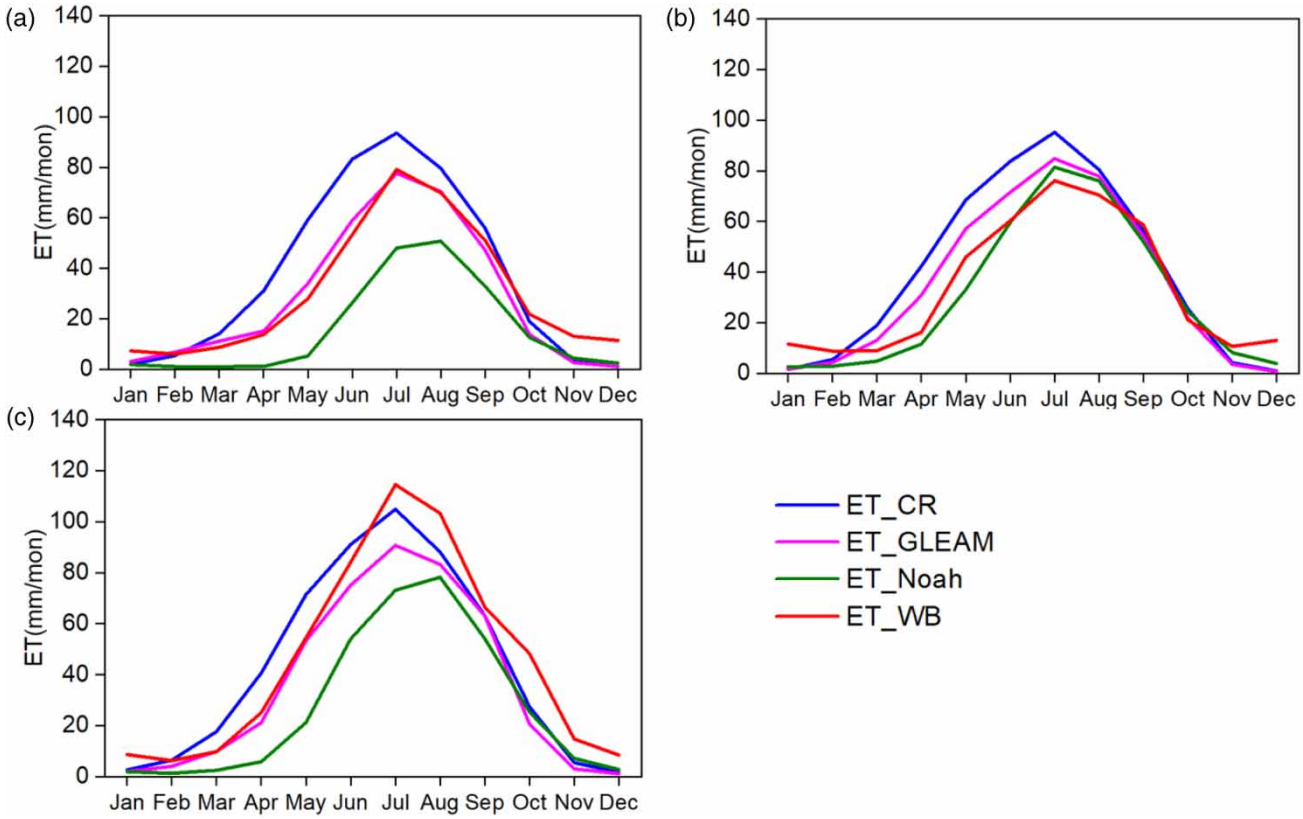

Figure 4 | Multi-year averages of monthly ET over (a) the SRYR, (b) the SRHR and (c) the SRLR during the period of 2003–2014. ET, Evapotranspiration; SRYR, Source region of the Yangtze River; SRHR, Source region of the Huang River; SRLR, Source region of the Lancang River. ET_WB represents monthly evapotranspiration estimated by the water balance method; ET_GLEAM represents monthly evapotranspiration derived from the Global Land Evaporation Amsterdam Model Version 3.3a product; ET_Noah represents monthly evapotranspiration derived from the Global Land Data Assimilation System with Noah Land Surface Version 2.0 product; ET_CR represents monthly evapotranspiration derived from the datasets simulated by the latest complementary relationship.

+1.15 mm/yr from 1960 to 2014 in the SRYR, which is consistent with the result (0.8 ± 0.4 mm/yr) estimated by this study. Annual ET in the SRLR has the highest variation range from 422 to 481 mm during the 1982–2014 period (Figure 5(c)). Meanwhile, a slightly decreasing trend in annual ET (-0.1 ± 0.5 mm/yr) has been observed in the SRLR during the entire study period. More information about the variation of annual ET over the study regions at monthly and seasonal scales is presented in Supplementary Figures S2 and S3, respectively.

5.4. Dominant drivers of annual ET across the TRSR

Global climate change has played a critical role in hydrological cycles and caused obvious variations in climatic variables over many parts of the world. For example, we can find an obvious increase in temperature for all three basins included

Table 4 | Weight w_i of each ET product during the 2003–2014 period based on the BMA approach

Category	SRYR	SRHR	SRLR
ET_CR	0.28	0.29	**0.41**
ET_GLEAM	**0.49**	0.34	0.38
ET_Noah	0.23	**0.37**	0.21

Note. The ET product with the highest value of weight w_i has been marked in bold. ET, Evapotranspiration; SRYR, Source region of the Yangtze River; SRHR, Source region of the Huang River; SRLR, Source region of the Lancang River. ET_WB represents monthly evapotranspiration estimated by the water balance method; ET_GLEAM represents monthly evapotranspiration derived from the Global Land Evaporation Amsterdam Model Version 3.3a product; ET_Noah represents monthly evapotranspiration derived from the Global Land Data Assimilation System with Noah Land Surface Version 2.0 product; ET_CR represents monthly evapotranspiration derived from the datasets simulated by the latest complementary relationship.

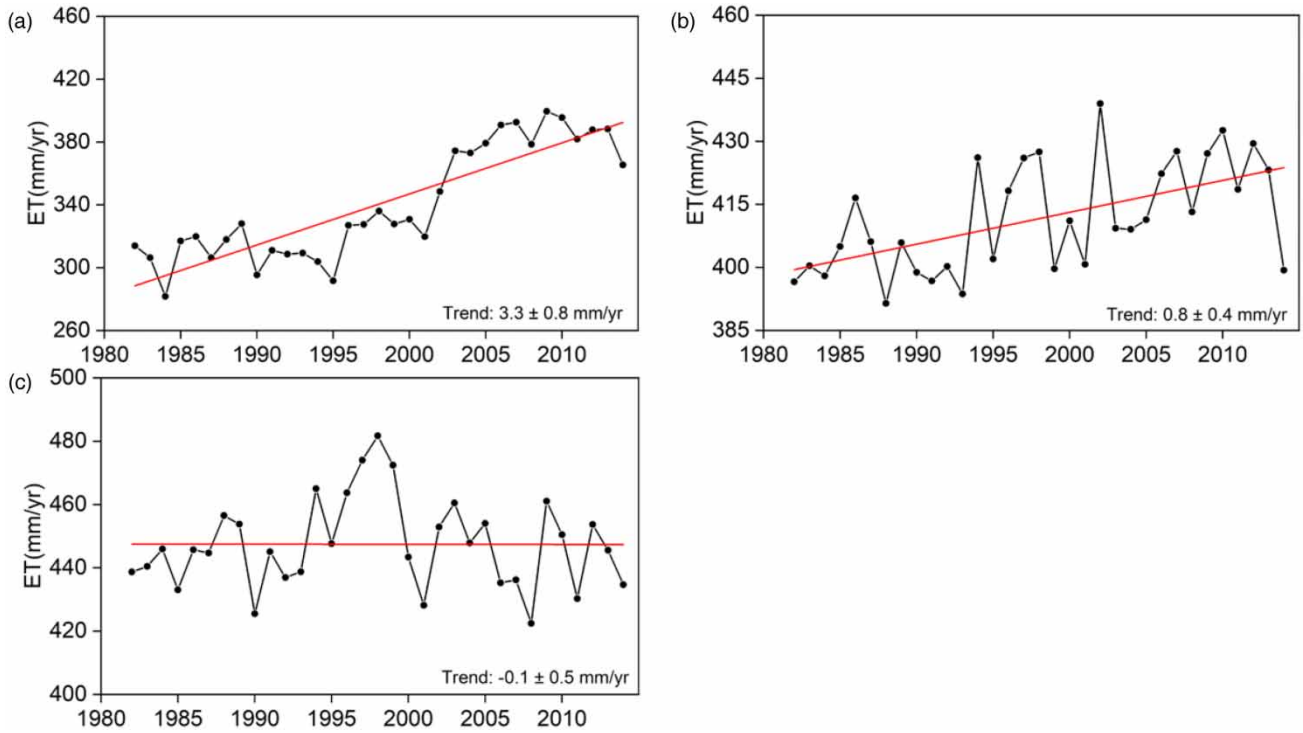

Figure 5 | Inter-annual variability of annual ET based on the BMA approach for (a) the SRYR, (b) the SRHR and (c) the SRLR during the 1982–2014 period. ET, Evapotranspiration; SRYR, Source region of the Yangtze River; SRHR, Source region of the Huang River; SRLR, Source region of the Lancang River; BMA, Bayesian model averaging.

in the entire TRSR (Supplementary Figure S4) during the past decades, especially in the SRYR and the SRHR. To assess the influences of climate change on ET, we further analyze the dominant drivers of annual ET across the TRSR based on the PLSR model. Table 5 shows the coefficients in the PLSR model, which can represent the sensitivity of long-term variation of annual ET to different climatic variables across the TRSR. A larger absolute value means greater importance of a specific climatic variable, while the sign of the coefficients suggests either positive or negative effect of the variable. For the SRYR, annual ET is more sensitive to precipitation and temperature with high coefficients above 0.50, while relative humidity and sunshine duration showed limited effects on annual ET. Li *et al.* (2014) suggested that annual mean precipitation correlated well with the annual mean ET across the SRYR, implying that increased precipitation was an important driving force for increasing trends in annual ET over this region.

For the SRHR, the coefficients of precipitation and temperature are obviously higher than the other climatic variables, implying that annual ET are mainly determined by precipitation and temperature. The above results are in line with the findings in previous studies. For example, Cong *et al.* (2009) indicated that variations in actual ET in the upper reaches of the Yellow River, which can be effectively calculated by a distributed hydrological model, were closely associated with precipitation. Liu & Yang (2010) found that precipitation was the main controlling factor for the annual series of actual ET in the upper mainstream section of the Yellow River Basin. In addition, Jiang *et al.* (2020) suggested that an increasing mean

Table 5 | Sensitivities of the long-term variations in annual ET to the climatic variables for three different basins included in the TRSR

Variables	SRYR	SRHR	SRLR
Relative humidity	−0.04	−0.15	**0.68**
Sunshine duration	0.08	0.18	0.21
Temperature	**0.51**	**0.29**	**0.65**
Precipitation	**0.58**	**0.32**	0.04

Note. Dominant drivers of the dynamics of ET in the specific region have been marked in bold. ET, Evapotranspiration; SRYR, Source region of the Yangtze River; SRHR, Source region of the Huang River; SRLR, Source region of the Lancang River.

temperature played an important role in ET increase in the west part of the Yellow River Basin (mainly refer to the SRHR) during 1981–2010.

For the SRLR, annual ET is most sensitive to relative humidity and precipitation during the study period (Table 5), which is slightly different from the other two regions. Using a remote sensing-based process model, Hu *et al.* (2021) also demonstrated that climate warming played a critical role in the ET variability for the upper reach of the Mekong River from 1980 to 2012. According to Ma *et al.* (2018), temperature and relative humidity can significantly influence the temporal pattern of potential evapotranspiration in the Lancang River Basin during the period of 1957–2015.

The above results also indicate that the dominant drivers of annual ET across the TRSR clearly vary from region to region. In general, temperature plays the most important role in inter-annual variations in ET among all climatic variables across all basins included in the TRSR. Meanwhile, precipitation is identified as the main driver for the observed increase in annual ET for the SRYR and the SRHR, while relative humidity is more sensitive to annual ET than the other climatic variables for the SRLR. This phenomenon can be explained by the strong discrepancies in climatic conditions as well as geophysical characteristics among all regions. Compared to previous studies (Xing *et al.* 2018; Li *et al.* 2019; Zhong *et al.* 2020), the method proposed in this study can successfully derive the long-term series of ET from 1982 to 2014 across the study region by integrating multiple sources of ET estimates, which makes full use of the strengths of land surface models and satellite-based products to constrain uncertainties. Meanwhile, the PLSR model can effectively address the problem of multi-collinearity among different variables when analyzing the sensitivities of annual ET to various climatic variables. As a result, our findings not only reveal the long-term dynamics of ET under climate change but also clearly show the influences of meteorological variables on those variations especially in high-mountain regions.

5.5. Uncertainties and limitations

In this study, the water balance method has been applied to estimate regional ET under the assumption that water exchange across the basin boundary could be negligible. The reliability of ET acquired from the water balance method largely depends on the accuracy of other hydrological variables included in the water balance equation (i.e., Equation (2); Li *et al.* 2019). Therefore, some measurement errors or uncertainty in these hydrological variables may result in a bias for ET over study regions. For example, traditional stream gauging stations only detect the variations of in-channel component of streamflow within the study regions but fail to provide important information on the exchange of groundwater stored in deep aquifers (Syed *et al.* 2005; Lv *et al.* 2017). This mismatch will inevitably lead to some differences between the actual ET for regions and that estimated by the water balance method.

As documented in previous studies (Sang *et al.* 2016; Zhang *et al.* 2020), accurate and reliable precipitation information are highly critical to understand the process of water exchange in high-mountain regions. Unfortunately, it has been challenging to obtain accurate precipitation estimation especially in less developed regions such as the TRSR. Limited meteorological stations can be regarded as an important source of uncertainties in the estimation of precipitation, which may significantly influence the final result of ET based on the water balance method. As a result, another two high-resolution precipitation products have been applied in this study with the goal of improving the accuracy of precipitation for regions. However, it still leads to uncertainty of precipitation, because rain gauges are unevenly and sparsely distributed over the study regions especially in the SRLR and the SRYR (shown in Figure 1).

When analyzing the relationships between ET and climatic variables, the PLSR model is a useful statistical method but cannot fully explain the inter-annual variations of ET over regions. In the context of future climate warming, tremendous changes are likely to take place in the hydrological cycle and ecological processes over the cold regions. Therefore, more attention still needs be paid to reveal the mechanism about how climate change influences ET variations in our next work.

6. CONCLUSION

Over the past decades, remarkable changes have taken place in the TRSR about ET under global climate change. However, sparse gauging networks and harsh environment have limited our knowledge about the variations of ET in some high-mountain regions, such as the TRSR of China. Accurate ET estimates in this region are critical not only for understanding regional water circulation but also for water resources management. The present study aimed to characterize the long-term dynamics of ET within the TRSR and explore the effects of changing climate on the hydrological cycle. The following conclusions can be drawn from this study:

(1) Various ET estimates for the TRSR were compared and the results showed that GLEAM for the SRYR (*KGE*=0.90), GLDAS NOAH for the SRHR (*KGE*=0.86) and CR for the SRLR (*KGE*=0.81) were most consistent with the water balance-derived ET estimates, showing the unique capability of gravity satellites in estimating regional ET combined with meteorological data.
(2) During 1982–2014, annual ET estimated by a BMA method was highest in the SRLR (422~481 mm) and followed by the SRHR (391~439 mm) but lowest in the SRYR (281~401 mm). Meanwhile, ET showed an upward trend at a rate of 3.3 ± 0.8 and 0.8 ± 0.4 mm/yr in the SRYR and the SRHR, respectively, whereas no significant trends were observed in the SRLR, indicating that hydrologic changes in response to climate change may vary from region to region.
(3) For the SRYR and the SRHR, annual ET was most sensitive to precipitation and temperature during the period of 1982–2014, while the other climatic variables (e.g., relative humidity and sunshine) showed limited effects in these regions. In comparison, temperature and relative humidity were the most important controlling factors that influenced the interannual variations of ET for the SRLR according to the PLSR model, which provided valuable information for understanding the effects of multiple driving factors on the hydrological process under climate change.

Overall, our findings have important implications for understanding the water-energy cycle in high-mountain regions in the context of global climate change. Moreover, variations in regional ET estimated by the water budget method can provide beneficial guidance for the management and assessments of local water resources. In future, more attention needs be paid to further explore the mechanism of how ET changes under multiple deriving factors when more accurate and detailed meteor-hydrological data are available.

ACKNOWLEDGEMENTS

This study was financially supported by the National Natural Science Foundation of China (52109037), the National Key Research and Development Program of China (2018YFC0407401) and the National Natural Science Foundation of China (91547106). The authors would like to thank the researchers and their teams for all of the data sets used in this study. We are grateful to China Meteorological Administration for providing the meteorological data (http://data.cma.cn/), the NASA MEaSUREs Program for providing JPL GRACE mascon solutions (https://grace.jpl.nasa.gov/data/get-data/jpl_global_mascons/), the Center for Space Research at the University of Texas at Austin for providing CSR GRACE mascon solutions (http://www2.csr.utexas.edu/grace/RL06_mascons.html), the Goddard Space Flight Center at NASA for providing GSFC GRACE mascon solutions (https://earth.gsfc.nasa.gov/geo/data/grace-mascons), the Goddard Earth Sciences (GES) Data and Information Services Center (DISC) of NASA for providing GLDAS Noah datasets (https://earthdata.nasa.gov/search?q=noah) and the National Tibetan Plateau Data Center for providing ET datasets (https://data.tpdc.ac.cn/zh-hans/). Furthermore, the GLEAM ET product was downloaded from the website (https://www.gleam.eu/), CGDPA precipitation data can be obtained from the website (http://data.cma.cn/) and PERSIANN-CDR precipitation data can be accessed at (ftp://data.ncdc.noaa.gov/cdr/persiann/files/). Runoff observations were provided by the Yellow River Conservancy Commission of Ministry of Water Resources (http://www.yellowriver.gov.cn/other/hhgb/) and the Yangtze River Water Resources Commission of Ministry of Water Resource (http://www.cjw.gov.cn).

DATA AVAILABILITY STATEMENT

All relevant data are available from an online repository or repositories. Meteorological data come from China Meteorological Administration (http://data.cma.cn/), GRACE data come from the Jet Propulsion Laboratory at NASA (https://grace.jpl.nasa.gov/data/get-data/jpl_global_mascons/), the Center for Space Research at the University of Texas at Austin (http://www2.csr.utexas.edu/grace/RL06_mascons.html) and the Goddard Space Flight Center at NASA (https://earth.gsfc.nasa.gov/geo/data/grace-mascons), GLDAS Noah datasets and ET datasets come from the Goddard Earth Sciences (GES) Data and Information Services Center (DISC) of NASA (https://earthdata.nasa.gov/search?q=noah), the GLEAM ET product was downloaded from the website (https://www.gleam.eu/), CGDPA precipitation data can be obtained from the website (http://data.cma.cn/) and PERSIANN-CDR precipitation data can be accessed at (ftp://data.ncdc.noaa.gov/cdr/persiann/files/), Runoff observations were provided by the Yellow River Conservancy Commission of Ministry of Water Resources (http://www.yellowriver.gov.cn/other/hhgb/) and the Yangtze River Water Resources Commission of Ministry of Water Resource (http://www.cjw.gov.cn).

REFERENCES

Abdi, H. 2007 Partial least square regression (PLS regression). In: *Encyclopedia of Measurement and Statistics* (Salkind, N. J., ed.). Sage Publications, Thousand Oaks, CA.

Afriyie, E., Verdoodt, A. & Mouazen, A. M. 2020 Estimation of aggregate stability of some soils in the loam belt of Belgium using mid-infrared spectroscopy. *Sci. Total Environ.* **744**, 140727.

Ashouri, H., Nguyen, P., Thorstensen, A., Hsu, K., Sorooshian, S. & Braithwaite, D. 2016 Assessing the efficacy of high-resolution satellite-based PERSIANN-CDR precipitation product in simulating streamflow. *J. Hydrometeorol.* **17** (7), 2061–2076. https://doi.org/10.1175/JHM-D-15-0192.1.

Awange, J. L., Fleming, K. M., Kuhn, M., Featherstone, W. E., Heck, B. & Anjasmara, I. 2011 On the suitability of the 4° × 4° GRACE mascon solutions for remote sensing Australian hydrology. *Remote Sens. Environ.* **115** (3), 864–875.

Baran, S., Hemri, S. & El Ayari, M. 2019 Statistical postprocessing of water level forecasts using Bayesian model averaging with doubly truncated normal components. *Water Resour. Res.* **55** (5), 3997–4013.

Billah, M. M., Goodall, J. L., Narayan, U., Reager, J. T., Lakshmi, V. & Famiglietti, J. S. 2015 A methodology for evaluating evapotranspiration estimates at the watershed-scale using GRACE. *J. Hydrol.* **523**, 574–586.

Bonnema, M. & Hossain, F. 2019 Assessing the potential of the Surface Water and Ocean Topography mission for reservoir monitoring in the Mekong River Basin. *Water Resour. Res.* **55**, 444–461. https://doi.org/10.1029/2018WR023743.

Chen, Y., Yuan, H., Yang, Y. & Sun, R. 2020 Sub-daily soil moisture estimate using dynamic Bayesian model averaging. *J. Hydrol.* **590**, 125445.

Chu, H., Wei, J., Qiu, J., Li, Q. & Wang, G. 2019 Identification of the impact of climate change and human activities on rainfall-runoff relationship variation in the Three-River Headwaters region. *Ecol. Indic.* **106**, 105516.

Cong, Z., Yang, D., Gao, B., Yang, H. & Hu, H. 2009 Hydrological trend analysis in the Yellow River basin using a distributed hydrological model. *Water Resour. Res.* **45** (7), W00A13.

Cui, J., Tian, L., Wei, Z., Huntingford, C., Wang, P., Cai, Z., Ma, N. & Wang, L. 2020 Quantifying the controls on evapotranspiration partitioning in the highest alpine meadow ecosystem. *Water Resour. Res.* **56** (4), e2019WR024815.

Duan, Q., Ajami, N. K., Gao, X. & Sorooshian, S. 2007 Multi-model ensemble hydrologic prediction using Bayesian model averaging. *Adv. Water Resour.* **30** (5), 1371–1386.

Gao, G., Chen, D., Xu, C. Y. & Simelton, E. 2007 Trend of estimated actual evapotranspiration over China during 1960–2002. *J. Geophys. Res.* **112**, D11120.

Hoeting, J. A., Madigan, D., Raftery, A. E. & Volinsky, C. T. 1999 Bayesian model averaging: a tutorial. *Stat. Sci.* **14** (4), 382–401. http://dx.doi.org/10.2307/2676803.

Hu, Z., Wang, G., Sun, X., Zhu, M., Song, C., Huang, K. & Chen, X. 2018 Spatial-temporal patterns of evapotranspiration along an elevation gradient on Mount Gongga, Southwest China. *Water Resour. Res.* **54**, 4180–4192. https://doi.org/10.1029/2018WR022645.

Hu, Z., Zhang, Z., Sang, Y. F., Qian, J., Feng, W., Chen, X. & Zhou, Q. 2021 Temporal and spatial variations in the terrestrial water storage across Central Asia based on multiple satellite datasets and global hydrological models. *J. Hydrol.* **2021**, 126013.

Immerzeel, W. W., Beek, L. P. H. & Bierkens, M. F. P. 2010 Climate change will affect the Asian water towers. *Science* **328**, 1382–1385.

Jiang, Z., Yang, Z., Zhang, S., Liao, C., Hu, Z., Cao, R. & Wu, H. 2020 Revealing the spatio-temporal variability of evapotranspiration and its components based on an improved Shuttleworth-Wallace model in the Yellow River Basin. *J. Environ. Manage.* **262**, 110310.

Landerer, F. W. & Swenson, S. C. 2012 Accuracy of scaled GRACE terrestrial water storage estimates. *Water Resour. Res.* **48** (4), W04531.

Lee, S., Yen, H., Yeo, I. Y., Moglen, G. E., Rabenhorst, M. C. & McCarty, G. W. 2020 Use of multiple modules and Bayesian Model Averaging to assess structural uncertainty of catchment-scale wetland modeling in a Coastal Plain landscape. *J. Hydrol.* **582**, 124544.

Lemordant, L., Gentine, P., Swann, A. S., Cook, B. I. & Scheff, J. 2018 Critical impact of vegetation physiology on the continental hydrologic cycle in response to increasing CO_2. *Proc. Natl. Acad. Sci.* **115**, 4093–4098. https://doi.org/10.1073/pnas.1720712115.

Li, X., Wang, L., Chen, D., Yang, K. & Wang, A. 2014 Seasonal evapotranspiration changes (1983–2006) of four large basins on the Tibetan Plateau. *J. Geophys. Res. Atmos.* **119**, 13079–13095.

Li, X., Long, D., Han, Z., Scanlon, B. R., Sun, Z., Han, P. & Hou, A. 2019 Evapotranspiration estimation for Tibetan Plateau headwaters using conjoint terrestrial and atmospheric water balances and multisource remote sensing. *Water Resour. Res.* **55** (11), 8608–8630.

Li, S., Wang, G., Sun, S., Hagan, D. F. T., Chen, T., Dolman, H. & Liu, Y. 2021a Long-term changes in evapotranspiration over China and attribution to climatic drivers during 1980–2010. *J. Hydrol.* **595**, 126037.

Li, Z., Li, Z., Feng, Q., Wang, X., Mu, Y., Xin, H., Song, L., Gui, J., Zhang, B., Gao, W., Xue, J., Li, Y., Yang, A., Nan, F., Liang, P. & Duan, R. 2021b Hydrological effects of multiphase water transformation in Three-River Headwaters Region, China. *J. Hydrol.* **601**, 126662.

Lian, X., Piao, S., Huntingford, C., Li, Y., Zeng, Z., Wang, X., Ciais, P., McVicar, T. R., Peng, S., Ottlé, C., Yang, H., Yang, Y., Zhang, Y. & Wang, T. 2018 Partitioning global land evapotranspiration using CMIP5 models constrained by observations. *Nat. Clim. Change* **8** (7), 640–646.

Liu, Q. & Yang, Z. 2010 Quantitative estimation of the impact of climate change on actual evapotranspiration in the Yellow River Basin, China. *J. Hydrol.* **395**, 226–234.

Liu, B., Hu, Q., Wang, W., Zeng, X. & Zhai, J. 2011 Variation of actual evapotranspiration and its impact on regional water resources in the Upper Reaches of the Yangtze River. *Quat. Int.* **244** (2), 185–193.

Liu, W., Wang, L., Zhou, J., Li, Y., Sun, F., Fu, G., Li, X. & Sang, Y. F. 2016 A worldwide evaluation of basin-scale evapotranspiration estimates against the water balance method. *J. Hydrol.* **538**, 82–95.

Liu, Z., Yao, Z., Wang, R. & Yu, G. 2020 Estimation of the Qinghai-Tibetan Plateau runoff and its contribution to large Asian rivers. *Sci. Total Environ.* **749**, 141570.

Long, D., Longuevergne, L. & Scanlon, B. R. 2013 Uncertainty in evapotranspiration from land surface modeling, remote sensing, and GRACE satellites. *Water Resour. Res.* **50**, 1131–1151. doi:10.1002/2013WR014581.

Long, D., Yang, Y., Wada, Y., Hong, Y., Liang, W., Chen, Y., Yong, B., Hou, A., Wei, J. & Chen, L. 2015 Deriving scaling factors using a global hydrological model to restore GRACE total water storage changes for China's Yangtze River basin. *Remote Sens. Environ.* **168**, 177–193. https://doi.org/10.1016/j.rse.2015.07.003.

Long, D., Pan, Y., Zhou, J., Chen, Y., Hou, X., Hong, Y., Scanlon, B. R. & Longuevergne, L. 2017 Global analysis of spatiotemporal variability in merged total water storage changes using multiple GRACE products and global hydrological models. *Remote Sens. Environ.* **192**, 198–216.

Lv, M., Ma, Z., Yuan, X., Lv, M., Li, M. & Zheng, Z. 2017 Water budget closure based on GRACE measurements and reconstructed evapotranspiration using GLDAS and water use data for two large densely-populated mid-latitude basins. *J. Hydrol.* **547**, 585–599.

Ma, R., Cai, C., Wang, J., Wang, T., Li, Z., Xiao, T. & Peng, G. 2015 Partial least squares regression for linking aggregate pore characteristics to the detachment of undisturbed soil by simulating concentrated flow in Ultisols (subtropical China). *J. Hydrol.* **524**, 44–52.

Ma, D., Wang, T., Gao, C., Pan, S., Sun, Z. & Xu, Y. P. 2018 Potential evapotranspiration changes in Lancang River Basin and Yarlung Zangbo River Basin, southwest China. *Hydrol. Sci. J.* **63** (11), 1653–1668.

Ma, N., Szilagyi, J., Zhang, Y. & Liu, W. 2019a Complementary relationship-based modeling of terrestrial evapotranspiration across China during 1982–2012: validations and spatiotemporal analyses. *J. Geophys. Res. Atmos.* **124**, 4326–4351. https://doi.org/10.1029/2018JD029850.

Ma, Y. J., Li, X. Y., Liu, L., Yang, X. F., Wu, X., Wang, P., Lin, H., Zhang, G. & Miao, C. 2019b Evapotranspiration and its dominant controls along an elevation gradient in the Qinghai Lake watershed, northeast Qinghai-Tibet Plateau. *J. Hydrol.* **575**, 257–268.

Madadgar, S. & Moradkhani, H. 2014 Improved Bayesian multimodeling: integration of copulas and Bayesian model averaging. *Water Resour. Res.* **50** (12), 9586–9603.

Martens, B., Miralles, D. G., Lievens, H., van der Schalie, R., de Jeu, R. A. M., Fernandez-Prieto, D., Beck, H. E., Dorigo, W. A. & Verhoest, N. E. C. 2017 GLEAM v3: satellite-based land evaporation and root-zone soil moisture. *Geosci. Model Dev.* **10** (5), 1903–1925.

Miralles, D. G., de Jeu, R. A. M., Gash, J. H., Holmes, T. R. H. & Dolman, A. J. 2011a Magnitude and variability of land evaporation and its components at the global scale. *Hydrol. Earth Syst. Sci.* **15** (3), 967–981.

Miralles, D. G., Holmes, T. R. H., de Jeu, R. A. M., Gash, J. H., Meesters, A. G. C. A. & Dolman, A. J. 2011b Global land-surface evaporation estimated from satellite-based observations. *Hydrol. Earth Syst. Sci.* **15** (2), 453–469.

Ndehedehe, C. E. & Ferreira, V. G. 2020 Assessing land water storage dynamics over South America. *J. Hydrol.* **580**, 124339.

Pan, Y., Zhang, C., Gong, H., Yeh, P. J.-F., Shen, Y., Guo, Y., Huang, Z. & Li, X. 2017 Detection of human-induced evapotranspiration using GRACE satellite observations in the Haihe River basin of China. *Geophys. Res. Lett.* **44**, 190–199. doi:10.1002/2016GL071287.

Pascolini-Campbell, M., Reager, J. T., Chandanpurkar, H. A. & Rodell, M. 2021 A 10 per cent increase in global land evapotranspiration from 2003 to 2019. *Nature* **593** (7860), 543–547.

Raftery, A. E., Gneiting, T., Balabdaoui, F. & Polakowski, M. 2005 Using Bayesian model averaging to calibrate forecast ensembles. *Mon. Weather Rev.* **113**, 1155–1174.

Ramillien, G., Frappart, F., Guntner, A., Ngoduc, T., Cazenave, A. & Laval, K. 2006 Time variations of the regional evapotranspiration rate from Gravity Recovery and Climate Experiment (GRACE) satellite gravimetry. *Water Resour. Res.* **42**, W10403. https://doi.org/10.1029/2005WR004331.

Rathinasamy, M., Adamowski, J. & Khosa, R. 2013 Multiscale streamflow forecasting using a new Bayesian Model Average based ensemble multi-wavelet Volterra nonlinear method. *J. Hydrol.* **507**, 186–200.

Reager, J. T. & Famiglietti, J. S. 2013 Characteristic mega-basin water storage behavior using GRACE. *Water Resour. Res.* **49**, 3314–3329. doi:10.1002/wrcr.20264.

Rodell, M., Houser, P. R., Jambor, U., Gottschalck, J., Mitchell, K., Meng, C. -J., Arsenault, K., Consgrove, B., Radakovich, J., Bosilovich, M., Entin, J. K., Walker, J. P., Lohmann, D. & Toll, D. 2004 The global land data assimilation system. *Bull. Am. Meteorol. Soc.* **85** (3), 381–394.

Sang, Y.-F., Singh, V. P., Gong, T., Xu, K., Sun, F., Liu, C., Liu, W. & Chen, R. 2016 Precipitation variability and response to changing climatic condition in the Yarlung Tsangpo River basin, China. *J. Geophys. Res. Atmos.* **121**, 8820–8831. doi:10.1002/2016JD025370.

Save, H., Bettadpur, S. & Tapley, B. D. 2016 High-resolution CSR GRACE RL05 mascons. *J. Geophys. Res. Solid Earth.* **121**, 7547–7569.

Shen, Y. & Xiong, A. 2016 Validation and comparison of a new gauge-based precipitation analysis over mainland China. *Int. J. Climatol.* **36** (1), 252–265. https://doi.org/10.1002/joc.4341.

Shen, Y., Xiong, A., Wang, Y. & Xie, P. 2010 Performance of high-resolution satellite precipitation products over China. *J. Geophys. Res.* **115**, D02114. https://doi.org/10.1029/2009JD012097.

Shen, S., Song, C., Cheng, C. & Ye, S. 2020 The coupling impact of climate change on streamflow complexity in the headwater area of the northeastern Tibetan Plateau across multiple timescales. *J. Hydrol.* **588**, 124996.

Shi, Z. H., Ai, L., Li, X., Huang, X. D., Wu, G. L. & Liao, W. 2013 Partial least-squares regression for linking land-cover patterns to soil erosion and sediment yield in watersheds. *J. Hydrol.* **498**, 165–176.

Shi, R., Yang, H. & Yang, D. 2020 Spatiotemporal variations in frozen ground and their impacts on hydrological components in the source region of the Yangtze River. *J. Hydrol.* **590**, 125237.

Soni, A. & Syed, T. H. 2021 Analysis of variations and controls of evapotranspiration over major Indian River Basins (1982–2014). *Sci. Total Environ.* **754**, 141892.

Sorg, A., Bolch, T., Stoffel, M., Solomina, O. & Beniston, M. 2012 Climate change impacts on glaciers and runoff in Tien Shan (Central Asia). *Nat. Clim. Change* **2** (10), 725–731.

Sun, R., Duan, Q. & Wang, J. 2021 Understanding the spatial patterns of evapotranspiration estimates from land surface models over China. *J. Hydrol.* **595**, 126021.

Syed, T. H., Famiglietti, J. S., Chen, J. L., Rodell, M., Seneviratne, S. I., Viterbo, P. & Wilson, C. R. 2005 Total basin discharge for the Amazon and Mississippi River basins from GRACE and a land-atmosphere water balance. *Geophys. Res. Lett.* **32**, L24404. https://doi.org/10.1029/2005GL024851.

Tang, Q., Zhang, X. & Tang, Y. 2013 Anthropogenic impacts on mass change in North China. *Geophys. Res. Lett.* **40**, 3924–3928. doi:10.1002/ grl.50790.

Wan, Z., Zhang, K., Xue, X., Hong, Z., Hong, Y. & Gourley, J. J. 2015 Water balance-based actual evapotranspiration reconstruction from ground and satellite observations over the conterminous United States. *Water Resour. Res.* **51** (8), 6485–6499.

Wang, J., Wang, Q., Zhao, Y., Li, H., Zhai, J. & Shang, Y. 2015 Temporal and spatial characteristics of pan evaporation trends and their attribution to meteorological drivers in the Three-River Source Region, China. *J. Geophys. Res. Atmos.* **120**, 6391–6408.

Wang, W., Li, J., Yu, Z., Ding, Y., Xing, W. & Lu, W. 2018 Satellite retrieval of actual evapotranspiration in the Tibetan Plateau: components partitioning, multidecadal trends and dominated factors identifying. *J. Hydrol.* **559**, 471–485.

Wöhling, T. & Vrugt, J. A. 2008 Combining multiobjective optimization and Bayesian model averaging to calibrate forecast ensembles of soil hydraulic models. *Water Resour. Res.* **44** (12), 1–18.

Xie, J., Xu, Y. P., Wang, Y., Gu, H., Wang, F. & Pan, S. 2019a Influences of climatic variability and human activities on terrestrial water storage variations across the Yellow River basin in the recent decade. *J. Hydrol.* **579**, 124218.

Xie, J., Xu, Y. P., Gao, C., Xuan, W. & Bai, Z. 2019b Total basin discharge from GRACE and Water balance method for the Yarlung Tsangpo River basin, Southwestern China. *J. Geophys. Res. Atmos.* **124**, 7617–7632.

Xie, J., Xu, Y. P., Guo, Y. & Wang, Y. 2021 Detecting the dominant contributions of runoff variance across the source region of the Yellow River using a new decomposition framework. *Hydrol. Res.* **52** (5), 1015–1032.

Xing, W., Wang, W., Shao, Q., Yong, B., Liu, C., Feng, X. & Dong, Q. 2018 Estimating monthly evapotranspiration by assimilating remotely sensed water storage data into the extended Budyko framework across different climatic regions. *J. Hydrol.* **567**, 684–695.

Xu, M., Kang, S., Chen, X., Wu, H., Wang, X. & Su, Z. 2018a Detection of hydrological variations and their impacts on vegetation from multiple satellite observations in the Three-River Source Region of the Tibetan Plateau. *Sci. Total Environ.* **639**, 1220–1232.

Xu, S., Yu, Z., Yang, C., Ji, X. & Ke, Z. 2018b Trends in evapotranspiration and their responses to climate change and vegetation greening over the upper reaches of the Yellow River basin. *Agric. For. Meteorol.* **263**, 118–129.

Xue, B. L., Wang, L., Li, X., Yang, K., Chen, D. & Sun, L. 2013 Evaluation of evapotranspiration estimates for two river basins on the Tibetan Plateau by a water balance method. *J. Hydrol.* **492**, 290–297.

Yan, B., Fang, N. F., Zhang, P. C. & Shi, Z. H. 2013 Impacts of land use change on watershed streamflow and sediment yield: an assessment using hydrologic modelling and partial least squares regression. *J. Hydrol.* **484**, 26–37.

You, Q., Chen, D., Wu, F., Pepin, N., Cai, Z., Ahrens, B., Jiang, Z., Wu, Z., Kang, S. & AghaKouchak, A. 2020 Elevation dependent warming over the Tibetan Plateau: patterns, mechanisms and perspectives. *Earth-Sci. Rev.* **210**, 103349. https://doi.org/10.1016/j.earscirev.2020.103349.

Yu, G. A., Brierley, G., Huang, H. Q., Wang, Z., Blue, B. & Ma, Y. 2014 An environmental gradient of vegetative controls upon channel planform in the source region of the Yangtze and Yellow Rivers. *Catena* **119**, 143–153.

Zhang, C. & Wang, Y. 2021 Controlling gully- and revegetation-induced dried soil layers across a slope-gully system. *Sci. Total Environ.* **755**, 142444.

Zhang, L., Ren, D., Nan, Z., Wang, W. & Wu, X. 2020 Interpolated or satellite-based precipitation? Implications for hydrological modeling in a meso-scale mountainous watershed on the Qinghai-Tibet Plateau. *J. Hydrol.* **583**, 124629.

Zhao, D. & Wu, S. 2019 Projected changes in permafrost active layer thickness over the Qinghai-Tibet Plateau under climate change. *Water Resour. Res.* **55**, 7860–7875.

Zhong, Y., Zhong, M., Mao, Y. & Ji, B. 2020 Evaluation of evapotranspiration for exorheic catchments of China during the GRACE era: from a water balance perspective. *Remote Sens.* **12**, 511.

Zhu, Q., Hsu, K., Xu, Y. & Yang, T. 2017 Evaluation of a new satellite-based precipitation data set for climate studies in the Xiang River basin, southern China. *Int. J. Climatol.* **37** (13), 4561–4575. https://doi.org/10.1002/joc.5105.

First received 10 July 2021; accepted in revised form 14 January 2022. Available online 3 February 2022